




ORIGINAL ARTICLE

The prometastatic relevance of tumor-infiltrating B lymphocytes in laryngeal squamous cell carcinoma

Francesco Missale^{1,2,3a} , Mattia Bugatti^{2,4}, Filippo Marchi^{1,5}, Giulio E Mandelli⁴, Maria Bruni⁴, Giulia Palmerini⁴, Matilde Monti² , Anna M Bozzola⁴, Giorgio Arena⁶, Luca Guastini^{1,5}, Maurizio Boggio¹, Giampiero Parrinello¹, Giorgio Peretti^{1,5a} & William Vermi^{2,4,7a} 

¹IRCCS Ospedale Policlinico San Martino, Genoa, Italy

²Department of Molecular and Translational Medicine, University of Brescia, Brescia, Italy

³Department of Head & Neck Oncology & Surgery Otorhinolaryngology, Antoni Van Leeuwenhoek, Nederlands Kanker Instituut, Amsterdam, The Netherlands

⁴Unit of Pathology, ASST Spedali Civili di Brescia, Brescia, Italy

⁵Department of Surgical Sciences and Integrated Diagnostics (DISC), University of Genoa, Genoa, Italy

⁶ENT Division, University of Easter Piedmont – AOU Maggiore della Carità di Novara, Novara, Italy

⁷Department of Pathology and Immunology, Washington University School of Medicine, MO, St. Louis, USA

Correspondence

F Missale and W Vermi, Department of Molecular and Translational Medicine, University of Brescia, Viale Europa, 11, 25123 Brescia, Italy.

E-mails: f.missale@unibs.it and william.vermi@unibs.it

^aEqual contributors.

Received 5 May 2022;

Revised 19 February 2023;

Accepted 28 March 2023

doi: 10.1002/cti2.1445

Clinical & Translational Immunology
2023; 12: e1445

Abstract

Objectives. Laryngeal squamous cell carcinomas (LSCCs) typically have an excellent prognosis for stage I tumors but a significant risk of locoregional and distant recurrence for intermediate to advanced disease. This study will investigate the clinical relevance of the tumor microenvironment in a large cohort of treatment-naïve patients affected by stage II–IV LSCC. **Methods.** Whole slide-based digital pathology analysis was applied to measure six immune cell populations identified by immunohistochemistry (IHC) staining for CD3, CD8, CD20, CD66b, CD163 and CD38. Survival analysis was performed by Cox proportional hazards models and unsupervised hierarchical clustering using the k-means method. Double IHC staining and *in-situ* hybridisation by RNAscope allowed further analysis of a protumoral B cell population. **Results.** A cohort of 98 patients was enrolled and analysed. The cluster of immune-infiltrated LSCCs demonstrated a significantly worse disease-specific survival rate. We also discovered a new association between high CD20⁺ B cells and a greater risk of distant recurrence. The phenotypic analysis of infiltrating CD20⁺ B cells showed a naïve (BCL6⁻CD27⁻Mum1⁻) regulatory phenotype, producing TGFβ but not IL10, according to an active TGFβ pathway, as proved by positive pSMAD2 staining. **Conclusion.** The identification of regulatory B cells in the context of LSCC, along with the activation of the TGFβ pathway, could provide the basis for new trials investigating the efficacy of already available molecules targeting the TGFβ pathway in the treatment of LSCC.

Keywords: B cells, Breg, laryngeal neoplasms, prognosis, tumor microenvironment

INTRODUCTION

One of the main objectives of modern precision oncology was to be able to predict outcomes and modulate treatment in individual patients by profiling the immune and molecular tumor landscape. During recent decades, various preclinical and clinical observations have established the crucial role of cancer immunosurveillance in controlling cancer growth.^{1–4} However, most clinically apparent and progressive human neoplasms have escaped cancer immunosurveillance, emerging as variants with reduced immunogenicity through an immunoediting process. As a result, a proportion of human cancers are immune deserts, whereas others are infiltrated by myeloid and lymphoid immune-suppressive cells.⁵ Extensive studies on colorectal carcinoma^{6,7} and other solid tumors^{8,9} have confirmed that the analysis of the tumor microenvironment (TME) enables the identification of patient subgroups with different prognoses and predicts the response to immune checkpoint inhibitors (ICI), such as immunotherapy.¹⁰ Among head and neck cancers, the recommendation of ICIs outside clinical trials is still limited to unresectable platinum-resistant tumors^{11,12} with an improved survival rate compared with standard of care; however, long-term, stable complete response is still unpredictable.¹³ The promising results of ICIs in neoadjuvant therapy could form the basis of a new clinical scenario for the treatment of these tumors.^{14–17} The identification of biomarkers of response is urgently needed to guide current and future therapeutic options. Recent analysis has revealed that head and neck squamous cell carcinomas (HNSCC) are highly mutated and distinct in molecular subtypes, including the HPV-driven subgroup showing improved prognosis.¹⁸ Given the high tumor mutational burden of HNSCC, neoantigen load could be an indicator of response to immunotherapies.¹⁹

Laryngeal squamous cell carcinoma (LSCC) is one of the most common HNSCCs with an overall estimate of 184 615 new cases and 99 840 new deaths in 2020. The clinical behaviour of stage I glottic tumors is favorable, with an excellent long-term prognosis²⁰; by contrast, the survival of patients with intermediate-advanced stage LSCC is still very poor.²¹ Specifically, in addition to locoregional recurrence, up to 15–20% of patients

develop hematogenous distant spread with limited treatment options and a median overall survival of 10 months.^{22,23} A few studies have analysed the TME of LSCCs and revealed that CD8⁺ T-cell infiltration is correlated with improved prognosis, whereas enrichment of tumor-infiltrating macrophages indicates LSCCs with poorer prognosis.^{24–29} No definitive data are available on the clinical relevance of tumor-infiltrating B cells, an immune population largely unexplored.^{24–29}

This study analyses the TME in a large retrospective cohort of LSCC. Ninety-eight treatment-naïve patients with intermediate-to-advanced stage tumors were included. Whole-slide digital pathology analysis was performed by counting six immune cell populations, namely CD3⁺ T cells, CD8⁺ T cells, CD20⁺ B cells, CD38⁺ plasma cells, CD66b⁺ neutrophils and CD163⁺ macrophages. Immune-enriched tumors were associated with a poorer disease-specific survival rate, supported by the multivariable analysis. Furthermore, our results identify an association between the density of tumor-infiltrating CD20⁺ B cells and a greater risk of distant recurrence. The in-depth analysis of this subgroup showed a naïve phenotype of B cells (BCL6[−], CD27[−] and Mum1[−]) and their localisation in a TGFβ-rich microenvironment, supporting the hypothesis of the presence of a regulatory B-cell (Breg) population in the immune contexture of LSCC.

RESULTS

Coordinated infiltration of immune cells in LSCC

Ninety-eight patients (PTs) were enrolled for this study including 83 men (84.7%) and 15 women (15.3%). The mean age at the time of the treatment was 67 years (range 43–89). In terms of surgical treatment, 62 PTs (63.3%) received transoral laser microsurgery (TLM), 14 (14.3%) open partial horizontal laryngectomies (OPHL) and 22 (22.4%) total laryngectomy (TL). According to the TNM staging system, 45 PTs (45.9%) were defined as pT2, 34 PTs (34.7%) as pT3 and 19 PTs (19.4%) as pT4a. Based on the regional lymph node involvement, 75 PTs (76.5%) were defined as N0, eight PTs (8.2%) as pN1, six PTs (6.1%) as pN2 and nine PTs (9.2%) as pN3. Risk factors such as perineural invasion (PNI) or lymphovascular

invasion (LVI) were identified in 44 (44.9%) and 38 (38.8%) PTs, respectively (Table 1). The median follow-up time was 49 months (95% CI 45–58 months). During the follow-up period, 25 (25.5%) PTs developed locoregional recurrence, whereas 15 (15.3%) PTs distant hematogenous metastases; 18 (18.4%) PTs died because of disease progression (Table 1).

Digital microscopy analysis was performed on immune-stained sections to quantify the tumor-associated CD3⁺ T cells, CD8⁺ T cells, CD20⁺ B cells, CD38⁺ plasma cells, CD66b⁺ neutrophils³⁰ and CD163⁺ macrophages (Figure 1a; Supplementary table 1). The median area of analysed tissue was 37.4 mm² (range 3.0–320.4 mm²; IQR 15.6–90.3 mm²). Using a cell recognition algorithm, the median densities of immune cells resulted, respectively, of 443 cells mm⁻² (range 68–2210 cells mm⁻²) for CD3⁺ T cells, of 457 cells mm⁻²

(range 30–3200 cells mm⁻²) for CD8⁺ T cells, of 178 cells mm⁻² (range 11–1230 cells mm⁻²) for CD20⁺ B cells, of 310 cells mm⁻² (range 5–2580 cells mm⁻²) for CD38⁺ plasma cells and of 140 cells mm⁻² (range 1–819 cells mm⁻²) for CD66b⁺ neutrophils. The CD163⁺ macrophages infiltrate, analysed with a pixel count algorithm, occupied a median area of 2.94% (range 0.005–18.29%) (Supplementary table 2).

Correlation analysis of the quantitative measurements of tumor-immune infiltrates, as performed by Spearman's correlation test, showed a strong direct correlation between all the immune cell populations analysed, with the exception of the CD66b⁺ cells (Figure 1b). Among the individual cells counted, CD3⁺ cells account for a median 46.4% of the immune infiltrate (range 9.5–85.4%), CD8⁺ a median 33.2% (range 3.4–85.4%), CD38⁺ a median 26.6% (range 0.3–65.9%), CD20⁺ a median 12.3% (range 1.9–51.3%) and CD66b⁺ a median 9.6% (range 0.1–63.4%) (Figure 1c; Supplementary table 3); for this analysis, CD163⁺ could not be included, as they were measured as a percentage of the tumor surface. At the individual tumor level, dimensionality reduction in immune infiltrates using the t-SNE method identified the coexistence of most of them and confirmed the independent enrichment of CD66b⁺ neutrophils (Figure 1d–i). Association analysis between clinical variables and immune cell infiltration did not any reveal any meaningful relationships (Supplementary tables 4–8).

Immune-infiltrated LSCCs reveal a phenotype of poorer prognosis

Considering the Z-score for immune cells infiltration, by the *average silhouette* method, the cohort can be best subdivided into two clusters (Figure 2a). Unsupervised *k-means* partitioning, as shown in Figure 2b, identified a dominant cluster (Cluster 1) characterised by Immune^{Cold} tumors and a minor cluster (Cluster 2) displaying enrichment of all the immune cells analysed (Immune^{Hot}). Cluster 2 was confirmed to be highly infiltrated by all the immune cells tested ($P < 0.05$; Figure 2c), whereas no correlation with the most relevant clinical features (pT category, pN involvement, PNI, LVI) was observed ($P > 0.05$, Supplementary table 9). Considering the survival end points in multivariable models including Age, pT category and pN category as covariates, Cluster

Table 1. Summary statistics of the cohort

Variable	Overall (N = 98)	Variable	Overall (N = 98)
Age		Cartilage invasion	
Mean (SD)	67.4 (9.82)	No	74 (75.5%)
Median [min, max]	67.0 [43.0, 89.0]	Yes	24 (24.5%)
Gender		N category	
Male	83 (84.7%)	N0	75 (76.5%)
Female	15 (15.3%)	N1	8 (8.2%)
Habits		N2	6 (6.1%)
None	7 (7.1%)	N3	9 (9.2%)
Smoke or alcohol	49 (50.0%)	ENE	
Both	42 (42.9%)	NO	75 (76.5%)
Site		N+ ENE–	13 (13.3%)
Glottis	55 (56.1%)	N+ ENE+	10 (10.2%)
Supraglottis	28 (28.6%)	Stage	
Transglottic	15 (15.3%)	Stage II	39 (39.8%)
Surgery		Stage III	33 (33.7%)
OPHL	14 (14.3%)	Stage IV	26 (26.5%)
TL	22 (22.4%)	Grading	
TLM	62 (63.3%)	G1	8 (8.2%)
Node dissection		G2	74 (75.5%)
No	50 (51.0%)	G3	16 (16.3%)
Yes	48 (49.0%)	PNI	
Margins		No	54 (55.1%)
Negative	68 (69.4%)	Yes	44 (44.9%)
Positive	30 (30.6%)	LVI	
T category		No	60 (61.2%)
pT2	45 (45.9%)	Yes	38 (38.8%)
pT3	34 (34.7%)		
pT4a	19 (19.4%)		

ENE, extranodal extension; LVI, lymphovascular invasion; OPHL, open partial horizontal laryngectomy; PNI, perineural invasion; TL, total laryngectomy; TLM, transoral laser microsurgery.

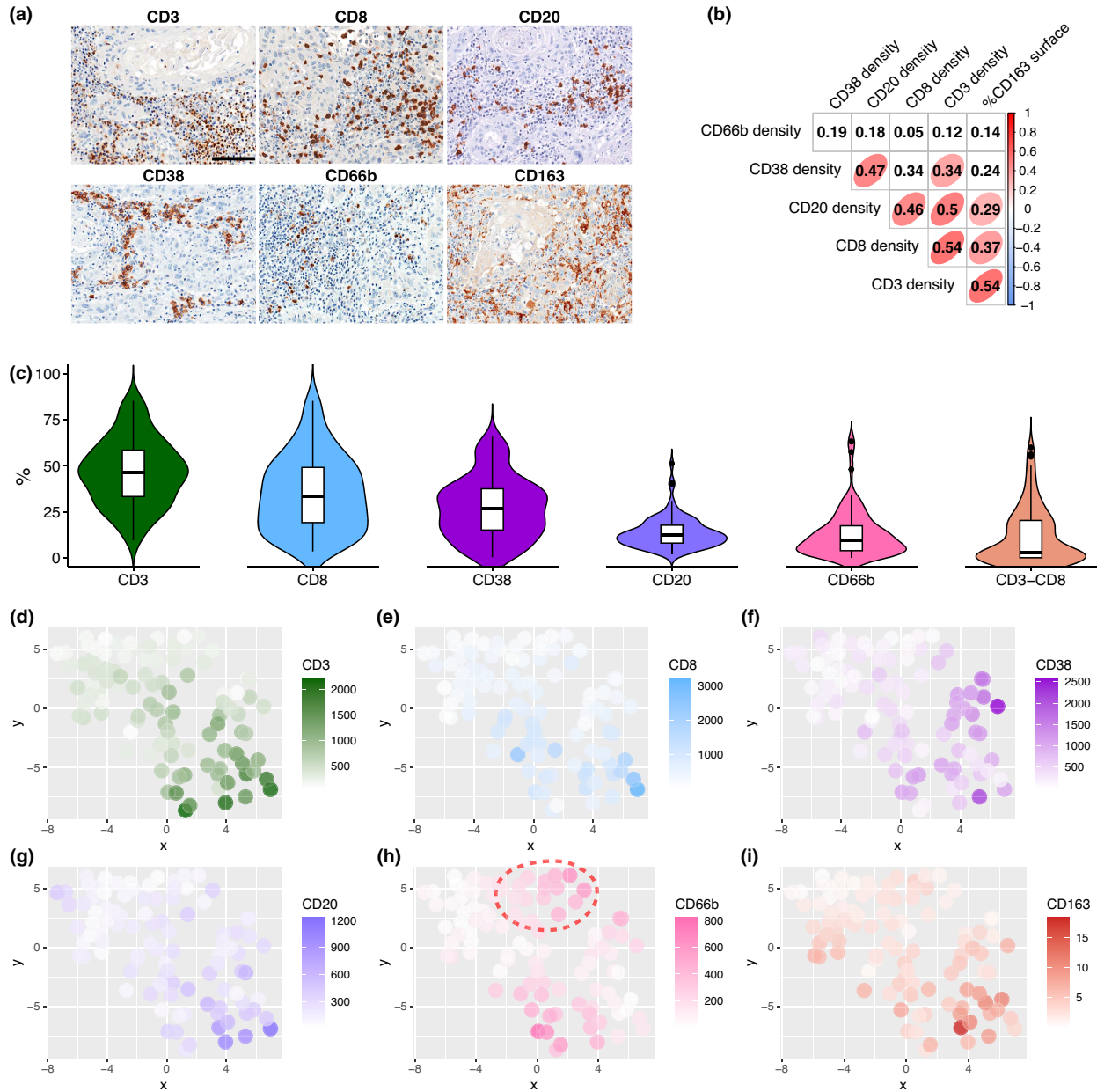


Figure 1. Representative immunohistochemical panel for immune cell quantification performed on laryngeal squamous cell carcinoma sections, scale bar 100 μ m (a). Spearman correlogram of immune cell density (b), *R* coefficient are shown and significant results, adjusted for multiple comparisons, are highlighted with coloured ellipses. Violin plots of relative fraction of immune cell densities (c). Plots of tSNE of z-scored immune cell density (d–i); a transversal immune-rich cluster can be identified, as well as one rich in CD66b⁺ cells (dotted red circle).

2 was independently associated with a poorer disease-specific survival rate (DSS) (HR 6.03; 95% CI 1.66–21.87; *P* = 0.006), as also shown in the adjusted survival curves in Figure 2d. The category pT4a showed a significant and independent risk factor (HR 25.81; 95% CI 5.35–124.45; *P* < 0.0001), as shown in Figure 2e and f combining its marginal effect with those of the clusters.

Dense infiltration by CD3⁺ T cells and CD20⁺ B cells indicates poor prognosis in LSCCs

The prognostic significance of each immune cell population was investigated separately, building a multivariable model for each outcome and evaluating the Akaike’s Information Criterion (AIC). As expected, the covariates Age, category

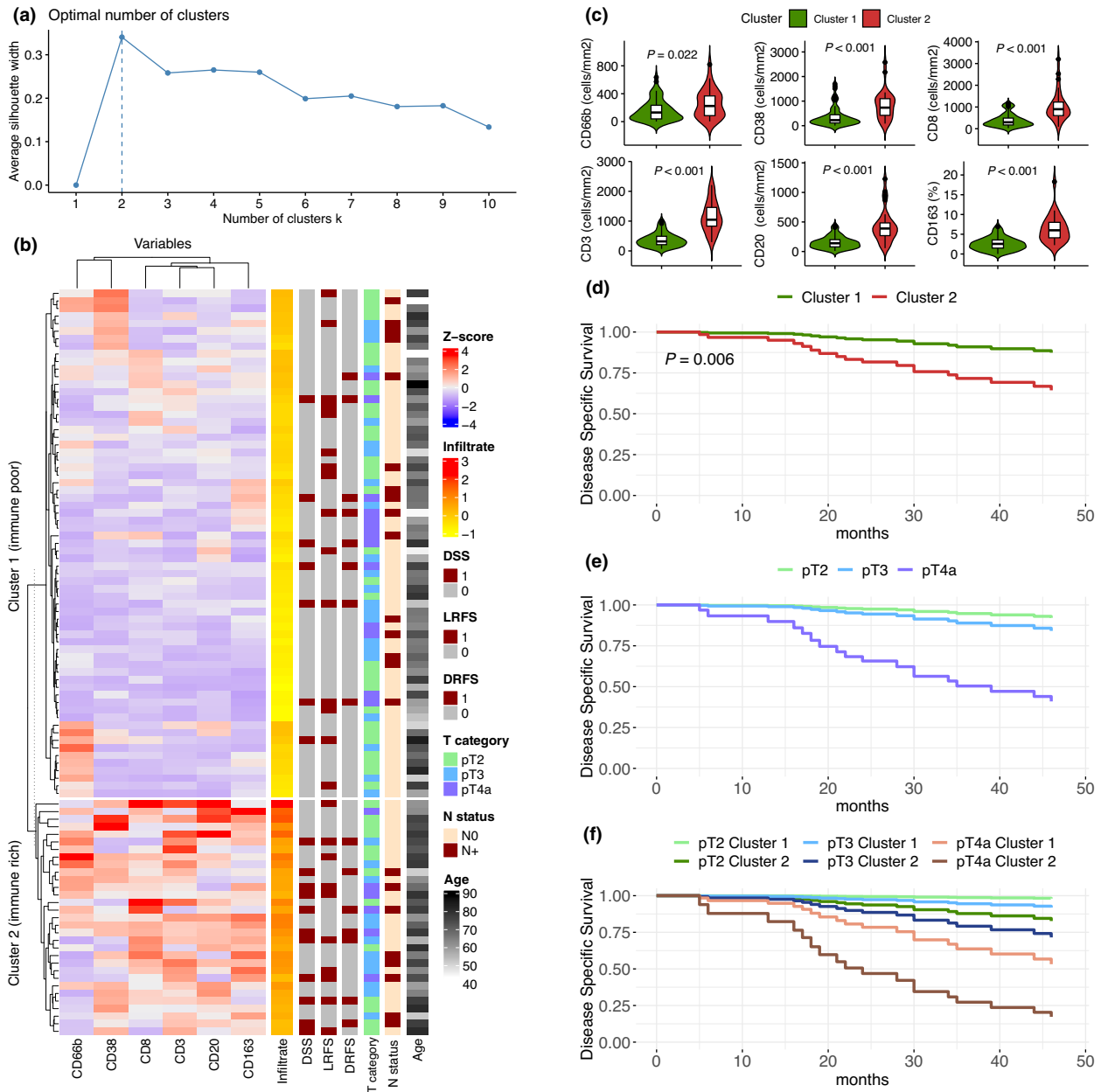


Figure 2. Maximising the average silhouette, considering the immune cell density, an optimum number of two clusters for *k*-means partitioning was identified **(a)**. Heatmap showing the *k*-means unsupervised clustering between samples, according to immune cell densities **(b)**; right annotations showing the average immune cell density, occurrence of survival endpoint events during follow-up and the main clinical features. Violin plots comparing immune cell densities among cluster 1 and cluster 2 identified by the *k*-means unsupervised clustering confirming that cluster 2 is enriched with all immune cells measured **(c)**. The multivariable model for DSS including as covariates Age, T category, N category and Clusters. Immune-rich cluster ($P = 0.006$), pT4 category ($P < 0.0001$) and Age ($P = 0.015$) were independent significant prognostic factors; the adjusted survival plots for the Cluster **(d)**, the pT category **(e)** and their combinations **(f)** is shown. DRFS, distant recurrence survival event; DSS, disease specific survival event; LRFS, locoregional recurrence free-survival event.

pT4a and LVI were strongly associated with the OS (Figure 3a).³¹ A non-linear effect was observed for the Age variable, being a risk factor at the lowest and highest value (Figure 3b). The CD3

density was retained in the model, but no association with the OS was observed. The DSS analysis confirmed Age and category pT4a as independent clinical covariates (Figure 3c); the

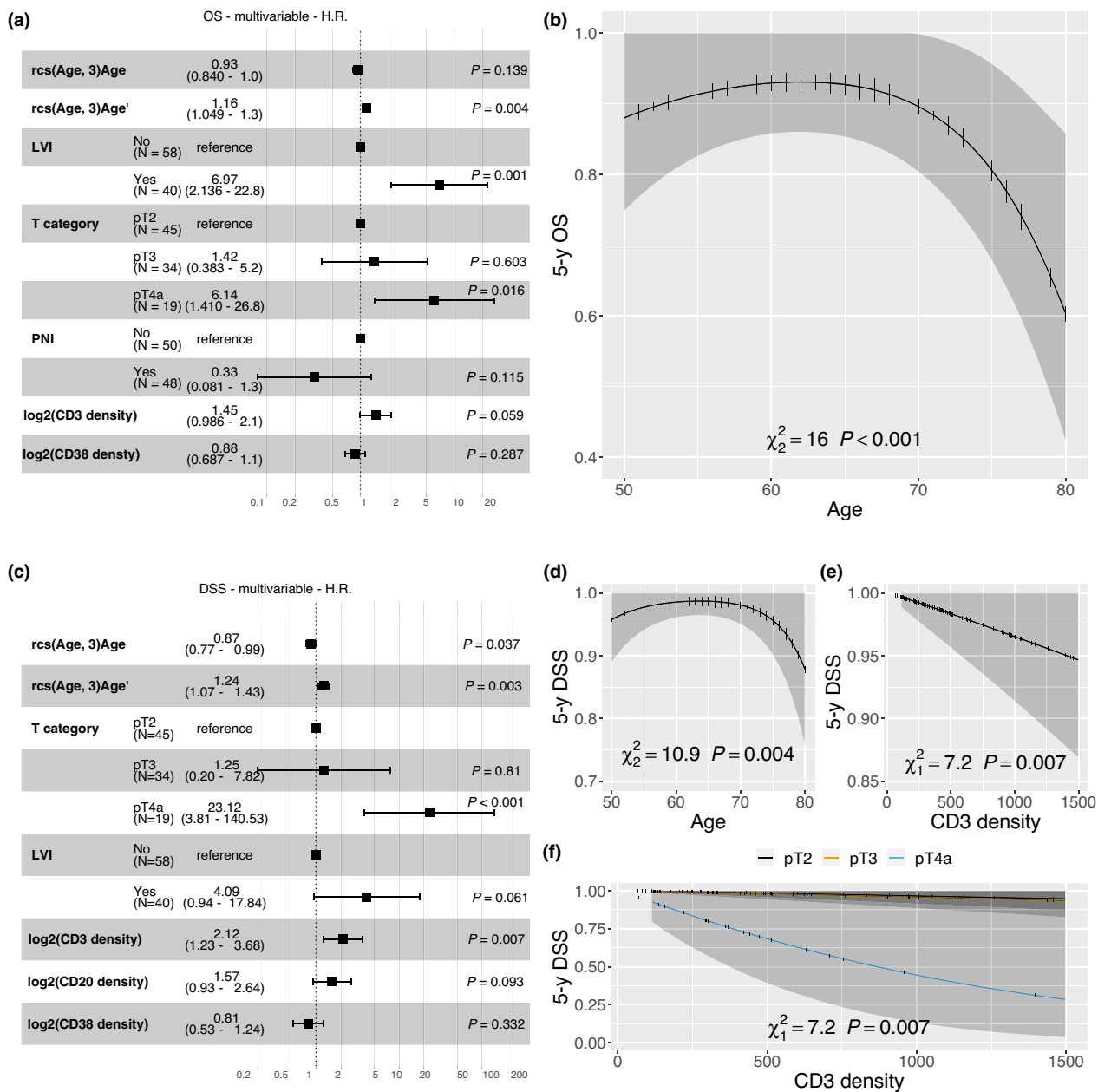


Figure 3. Forest plot of the multivariable overall survival rate (OS) model **(a)**. Plot showing the adjusted effect of Age on the 5-year OS probability derived from the multivariable OS model **(b)**. Forest plot of the multivariable disease specific survival rate (DSS) model **(c)**. Plots showing the adjusted effect of Age **(d)**, CD3⁺ T-cell density **(e)** and the combined effect of CD3⁺ T-cell density and pT category **(f)** on the 5-year DSS probability derived from the multivariable DSS model. As age variable is modelled with a restricted cubic spline with three knots, in each model is shown the linear term (Age) and the not-linear one (Age').

effect of Age followed a non-linear shape, as for OS (Figure 3d). The CD3 density represented a risk factor (Figure 3e and f) with an HR of 2.12 for each doubling of the CD3 density value (95% CI 1.23–3.68; $P = 0.007$), consistent with the result showing the detrimental prognostic role of Cluster 2. Notably, when considering locoregional

recurrence-free survival (LRFS), CD3 density was the only covariate independently associated with this outcome (Figure 4a) in the form of risk factor with an HR of 1.73 for each doubling value (95% CI 1.17–2.7; $P = 0.014$; Figure 4b and c). Interestingly, a significant interaction was observed between the density of CD3⁺ and pT

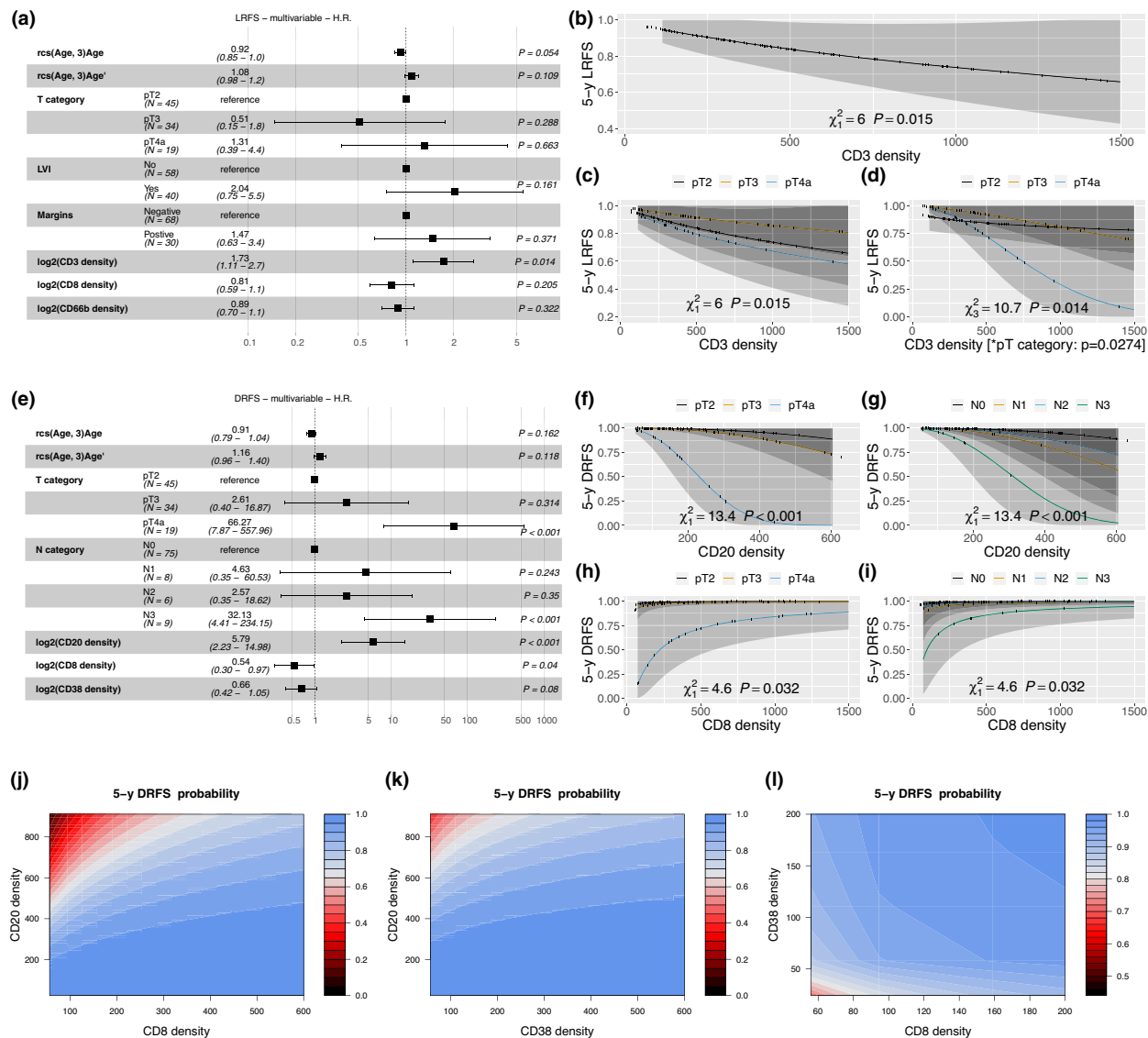


Figure 4. Forest plot of the multivariable locoregional recurrence free survival rate (LRFS) model (a). Plots showing the adjusted effect of CD3⁺ T-cell density (b) and its paired effect with pT category (c) derived from the multivariable LRFS model and their effect including their significant interaction term (d) in the model. Forest plot of the multivariable distant recurrence free survival rate (DRFS) model (e). Plots showing the adjusted effect of CD20⁺ B-cell density combined with pT category (f) or N-category (g) derived from the multivariable DRFS model. Plots showing the adjusted effect of CD8⁺ T-cell density combined with pT category (h) or N-category (i) derived from the multivariable DRFS model. Contours plots showing the 5-year DRFS probability considering together the CD8⁺ T-cell and CD20⁺ B-cell densities (j), the CD38⁺ plasmacell and CD20⁺ B-cell densities (k) and the CD8⁺ T-cell and the CD38⁺ plasma cell densities (l). As age variable is modelled with a restricted cubic spline with 3 knots, in each model is shown the linear term (Age) and the not-linear one (Age').

category ($P = 0.0274$), as shown in Figure 4d, with a remarkable effect on prognosis in the pT4a group, as seen for the DSS.

Analysing the distant recurrence-free survival (DRFS) as an oncological outcome, categories pT4a and N3 were both associated with a poorer prognosis ($P < 0.001$), compared with the reference categories (pT2 and N0). Among tumor-

infiltrating immune cells, a higher density of CD20⁺ B cells was associated with a worse outcome (HR 5.79; 95% CI 2.23–14.98; $P < 0.001$), whereas enrichment of CD8⁺ T cells resulted protective (HR 0.54; 95% CI 0.30–0.97; $P = 0.04$; Figure 4e–i). Contour plots in Figure 4j–l illustrate the combined effects of each immune cell density measure in the model, to predict the 5-year DRFS.

Occurrence and localisation of CD20⁺ B cells in LSCC

The evidence of the poorer prognosis indicated by CD20⁺ B-cell infiltration led to an in-depth analysis of their localisation within the TME. The B cells were organised into aggregates (median, 36.0%; min–max, 0–83.7%) also identifiable as tertiary lymphoid structures (TLS), based on the occurrence of BCL6⁺ germinal centre B cells (CD20^{TL5}); alternatively, CD20⁺ B cells occur as diffuse stromal/intratumoral infiltrate (CD20^{IT}) (median, 64.0%; min–max, 16.3–100%). The frequency of TLS – in TLS per square millimetre – was also taken into account, with a median value of 0.131 TLS mm⁻² (min–max, 0.010–2.32 TLS mm⁻²) for the whole cohort. The density of CD20⁺ B cells measured in the different areas of interest (CD20^{TL5} and CD20^{IT}) showed strong, direct correlation ($P < 0.0001$, Figure 5a–c), suggesting a coordinated recruitment of B cells occurring as TLS or diffuse into the tumor/stroma. A significant decrease in TLS was observed in advanced T and N categories, along with the progression of the disease, and a significant decrease in TLS density was also observed for tumor-harboring risk factors, such as PNI and/or LVI (Figure 5d and e). A further multivariable model was fitted to analyse the clinical relevance of CD20^{TL5} and CD20^{IT} in terms of distant recurrence. Adding the TLS density as covariate did not result in any improvement in the regression model (AIC_{pre} 102.68, AIC_{post} 104.35), and this variable was not even associated with a variation in DRFS (HR 1.26; 95% CI 0.574–2.763; $P = 0.5647$, Figure 5f–i), still being the whole CD20⁺ density a significant risk factor (HR 5.053; 95% CI 1.771–14.419; $P = 0.002$, Figure 5f–i). Thus, the enrichment of CD20⁺ B cells, and not their differential localisation, is relevant for the risk of distant recurrence in LSCC.

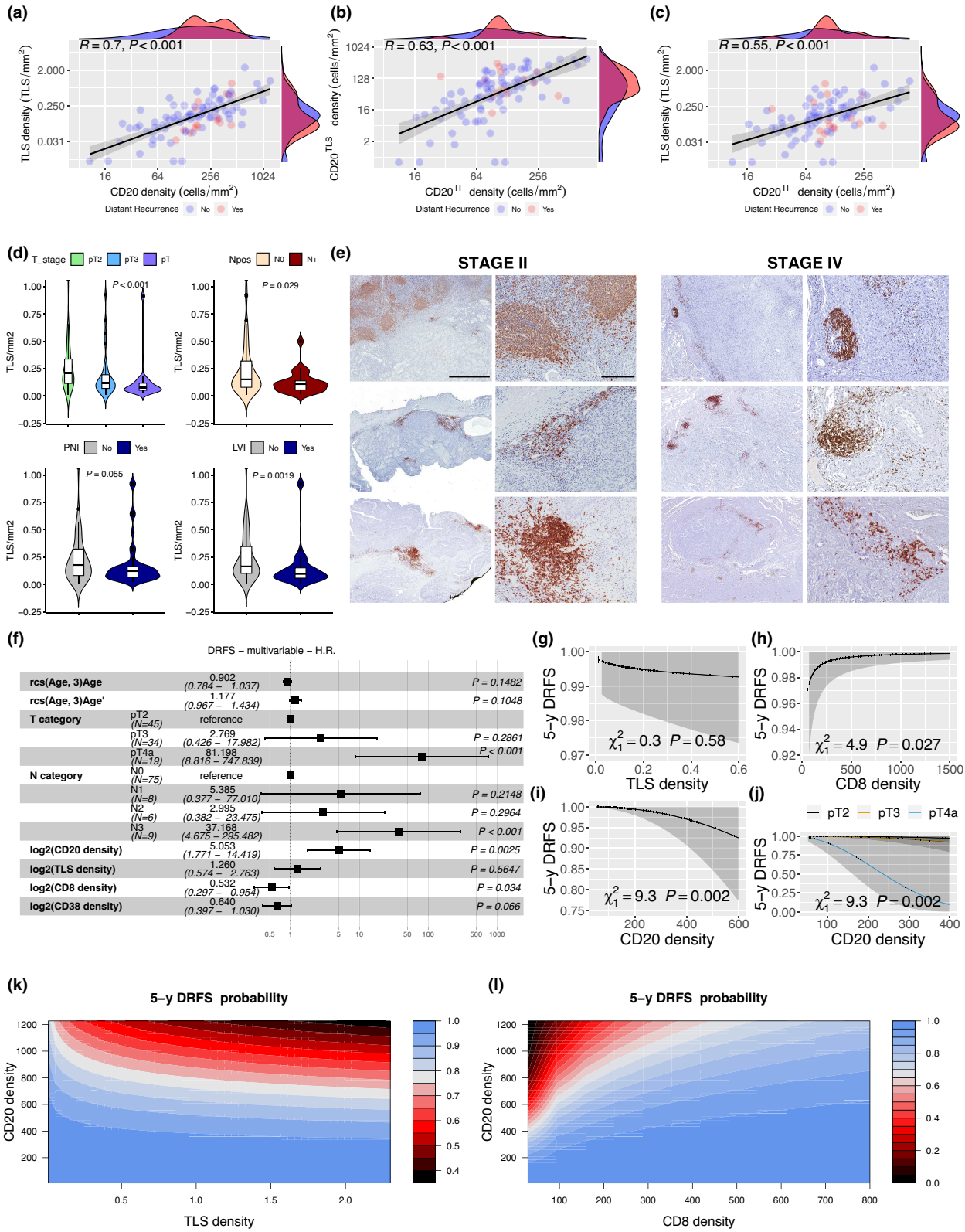
In-situ characterisation of prometastatic B cells

Tumor-infiltrating B cells are in general poorly characterised and data on head and neck squamous cell carcinoma are limited to the oral cavity, oropharynx and hypopharynx sites,³² with studies on the laryngeal site included in mixed cohorts.²⁶ Data in the literature show that B cells can be localised both in the tumoral or in the stromal compartment, and they often contribute to the composition of TLS, although their exact function and clinical relevance are not yet completely understood.³³ To investigate the phenotype of CD20^{IT} B cells, we tested a set of B-cell antigens – including CD20, Pax5, Bcl6, Mum1 and CD27 – on serial and double-stained sections of a set of cases that experienced distant recurrence during the follow-up period ($n = 15$).^{34,35} The TLS – defined as aggregates of B and T cells showing a BCL6⁺ germinal centre phenotype – were excluded from this analysis (Figure 6a and b). Based on double stains, we found that most CD20^{IT} lacked CD27 (median fraction of CD27⁺/CD20⁺ < 1%) and Mum1 reactivity (median fraction of MUM1⁺/CD20⁺ < 1%), thus corresponding to mature B cells with naïve phenotype lacking plasma cell differentiation (Figure 6c).^{34,35}

Functional analysis of prometastatic B cells

To extend our analysis at the functional level, we tested the expression of IL-10 and TGFβ by using RNAscope on a subset of the cases that experienced distant recurrence during the follow-up period ($n = 13$). IL-10 and TGFβ probes were validated in cell-blocks of monocyte-derived macrophages showing – as expected – a selective expression of IL-10 on M2 macrophages and a diffuse expression of TGFβ both on M1 and M2

Figure 5. Scatter plots showing the significant direct correlation between CD20⁺ B-cell density and TLS density (a), between CD20^{IT} B-cell density and CD20^{TL5} B-cell density (b) and between CD20^{IT} B-cell density and TLS density (c). Violin plots showing the significant decrease in density of clusters of B cells as the disease progresses (d) considering both pT category, nodal involvement, and presence of risk factors as perineural invasion and lymphovascular invasion. Sections from representative Stage II ($n = 3$) or Stage IV ($n = 3$) laryngeal squamous cell carcinoma cases immunostained as labelled (e), first and third column scale bar 1 mm, second and fourth column scale bar 200 μm. Forest plot of the multivariable distant recurrence-free survival rate (DRFS) model including density of B cells as covariate (f). Plots showing the adjusted insignificant effect of the density of B-cell clusters (g) and the significant effect of clusters of CD8⁺ T cells (h) and CD20⁺ B cells (i, j). Contour plots showing the 5-year DRFS probability strongly associated with CD20⁺ B-cell (k) and CD8⁺ T-cell (l) densities and not with the density of B-cell clusters. As age variable is modelled with a restricted cubic spline with 3 knots, in each model is shown the linear term (Age) and the non-linear one (Age²).



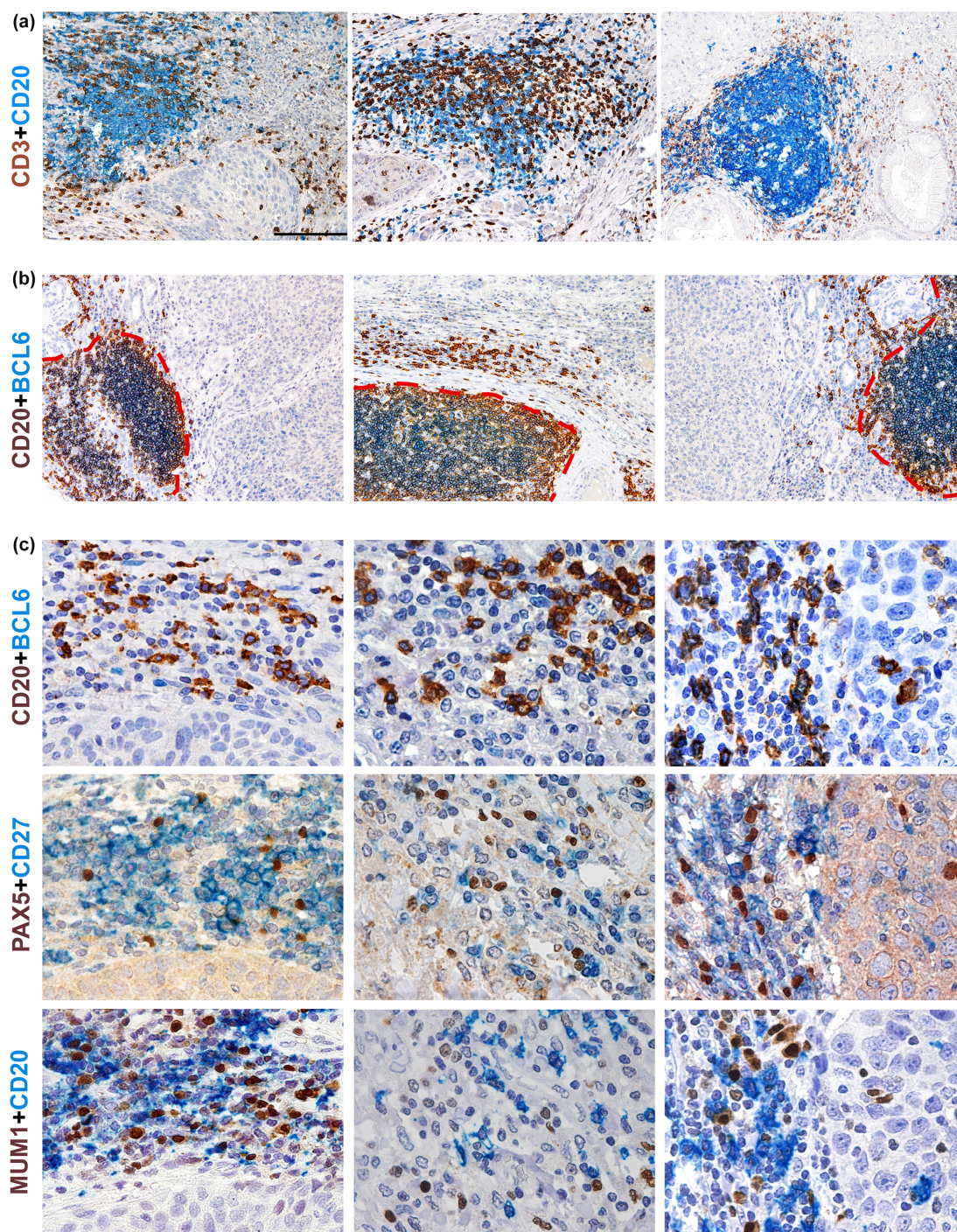


Figure 6. Sections from laryngeal squamous cell carcinoma (LSCC) cases that experienced distant recurrence ($N = 15$) stained as labelled showing the *in-situ* characterisation of pro-metastatic B cells; slides in each column belong to the same LSCC case ($N = 3$). **(a)** Double immunohistochemistry (IHC) for CD3 and CD20 for the identification of TLS ($N = 3$); magnification 100 \times , scale bar 200 μm . **(b)** Areas of interest outside the TLS (outside the dotted red lines); TLS are identified by double IHC for CD20 and BCL6 ($N = 3$); magnification 100 \times . Scale bar 200 μm . **(c)** Representative high-power fields of serial sections double stained for CD20/BCL6, PAX5/CD27, MUM1/CD20; B cells (CD20^+ or PAX5^+) result largely negative for CD27 and MUM1, defining a B-cell mature naïve phenotype ($N = 3$); magnification 400 \times . Scale bar 50 μm .

macrophages; this observation was also validated by RT-qPCR data (Supplementary table 2, not shown).

Based on RNAscope findings, TGF β mRNA resulted strongly and diffusely expressed by tumor cells and TME cells (mean \pm SD scores 1.6 ± 1.0 and 2.2 ± 0.8 on a scale of 0–3; Figure 7a), whereas IL-10 expression was limited to the TME compartment (Figure 7a). Specifically, by using a set of immunohistochemical markers, we found that among TME cells, TGF β transcript were detected in CD20^T, CD163⁺ macrophages and SMA⁺ fibroblasts (Figure 7b), whereas IL-10 expression was limited to CD163⁺ macrophages (Figure 7b). Furthermore, by triple immunohistochemical staining for FOXP3, CD20 and CD3 or CD8, we demonstrated recurrent cell interaction between CD20^T and CD3⁺FOXP3⁺ T cells, the latter displaying a CD8⁻CD3⁺ Treg phenotype (Figure 7c; Supplementary table 3). Thus, our data support the identification in LSCC of a subset of naïve CD20^T TGF β ⁺ consistent with the ‘tumor-evoked’ regulatory B cells (tBregs), previously identified as promoters of breast cancer metastasis through the conversion of resting CD4⁺ T cells to regulatory T cells.³⁶ Furthermore, testing for pSMAD2 reactivity, nuclear positivity was observed in most of the tumor-infiltrating CD20⁺ B cells (TIBs) in such cases and on tumor cells, further supporting the activation at least of the TGF β pathway (Figure 7d). It has been reported that IL-10⁺ Bregs can also express PD-L1, showing that the PD-1/PD-L1 pathway is involved in their immune suppressive function; by contrast the phenotype of TGF β ⁺ Bregs has been poorly characterised.³⁷ By double immunohistochemistry, we found that PAX5⁺ B cells regularly resulted negative for PD-L1 ($n = 15$). Overall, the phenotype of prometastatic TIBs is consistent with a TGF β ⁺-producing Breg population (Figure 7e).

DISCUSSION

In the present study, we have characterised the TME of a homogeneous retrospective cohort of patients affected by LSCC and surgically treated at a referral center. The relevant findings included a significantly worse DSS for a cluster of immune-infiltrated cases (Immune^{Hot}), representing one-third of the cohort, as confirmed in multivariable analysis. Furthermore, the investigation of different survival outcomes identified a correlation between high CD20⁺ B-cell density and

an increase in distant recurrence. The immunophenotype of the intratumoral CD20⁺ B cells was consistent with a naïve B-cell phenotype with production of TGF β , likely corresponding to regulatory B phenotype.

Studies on colorectal carcinoma,^{6,38} subsequently extended to other cancer types,⁸ have shown that the type and density of immune cells in the TME are among the key prognosticators of the clinical outcomes of patients, beyond the classical staging criteria.³⁹ The available literature on LSCC TME is limited to few studies based on tissue microarray samples and computing only OS and DFS as outcomes.^{24–29,40,41} Most authors confirmed the positive prognosis associated with high CD8⁺ T-cell density,^{24,26,28,29} as was also observed in our analysis of distant recurrence. The positive association with high CD8⁺ T-cell density was already proved by a meta-analysis by Rodrigo *et al.*⁴² considering both overall and disease-free survivals as outcomes. However, as one of the main findings of this study, we identified an association between an immune-rich TME and a poorer DSS. Although surprising, this observation is not limited to our cohort. Höing *et al.*²⁵ observed a poorer OS in LSCC patients with high CD45⁺ cell infiltration; similar observations were made for cohorts of renal clear cell carcinoma.^{9,43,44} One possible explanation for this finding is the exhaustion of T cells in the TME as the tumor progresses^{44,45}; this is also consistent with the observed significant interaction between CD3⁺ T-cell density and T stage in the survival analysis in the present study. These hypotheses are supported by recent observations,⁴² including the analysis on the HNSCC cohort of the ‘The Cancer Genome Atlas’ (TCGA) data set.⁴⁶

The investigation in our cohort of different survival outcomes identified a population of CD20⁺ B cells in the tumoral area associated with an increase in distant recurrence. Previous findings in the HNSCC literature also support this observation. Whole genome expression analysis in a matched cohort of 49 patients suffering primary HNSCC showed an enrichment of plasma cells and T-reg-estimated with a deconvolution algorithm in the group that experienced distant recurrence.⁴⁷ Data on the clinical and biological relevance of TIB in the immune contexture of solid tumors are limited.⁴⁸ The emerging literature – mostly derived from the analysis of cohorts of patients treated with immunotherapy – suggests

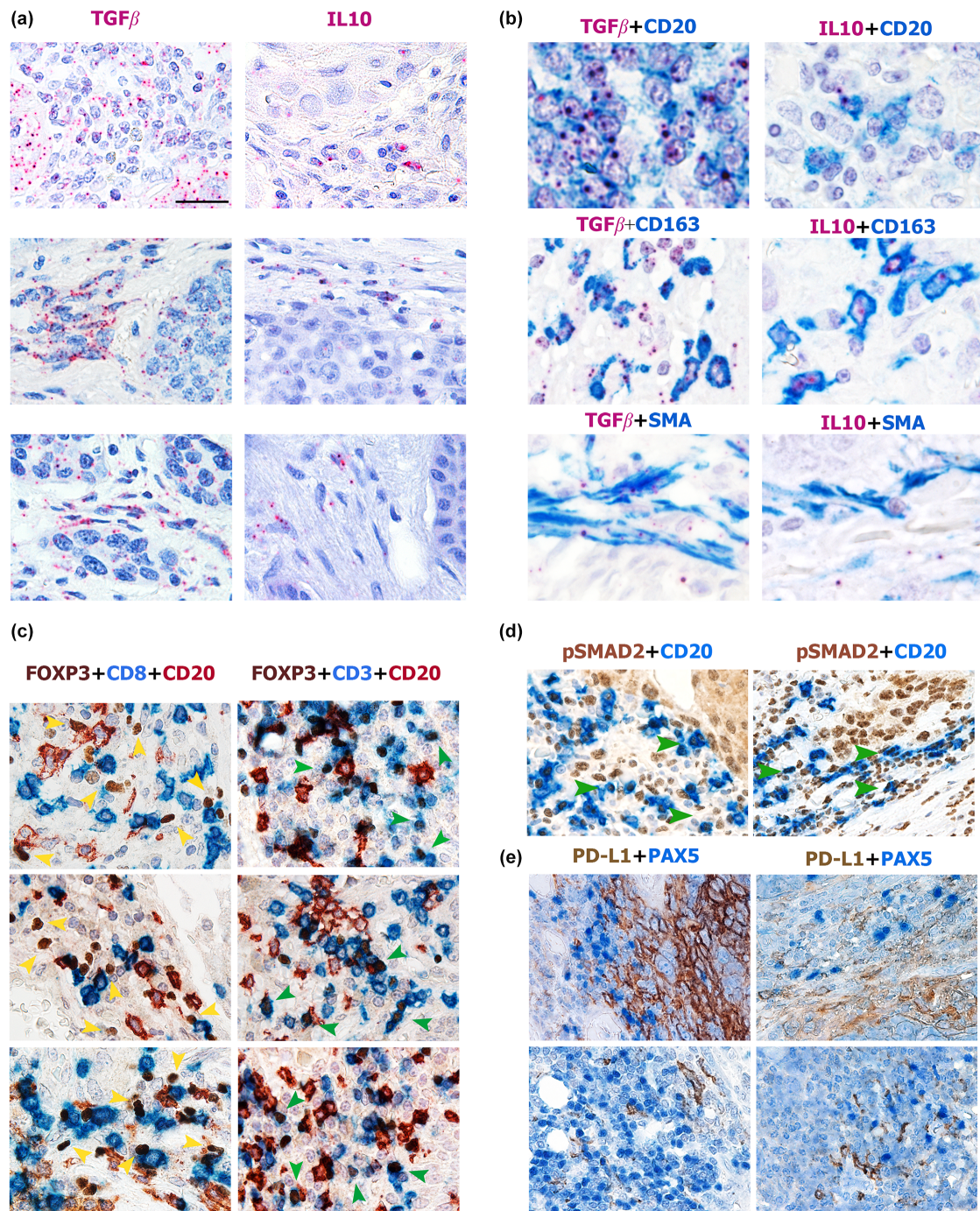


Figure 7. Sections from laryngeal squamous cell carcinoma (LSCC) cases that experienced distant recurrence ($N = 15$) and stained as labelled. **(a)** *In situ* hybridisation for TGF β and IL-10 using RNAscope is shown ($N = 3$); magnification 400 \times scale bar 50 μ m. **(b)** *In situ* hybridisation for TGF β and IL-10 is combined with immunohistochemistry for CD20, CD163 and SMA and confirm the positivity of TGF β on CD20 $^+$ B cells, CD163 $^+$ macrophages and on SMA $^+$ tumor-associated fibroblasts; conversely, IL-10 expression is limited to CD163 $^+$ macrophages; magnification 600 \times scale bar 33 μ m. **(c)** Co-localisation of CD20 $^+$ B cells together with CD3 $^+$ T regs (CD3 $^+$ FOXP3 $^+$ CD8 $^-$); FOXP3 reactivity is found on CD3 $^+$ (green arrowhead) CD8 $^-$ (yellow arrowhead) cells ($N = 3$); magnification 400 \times scale bar 50 μ m. **(d)** Double staining for pSMAD2 and CD20 confirmed the activation of TGF β pathway in a relevant fraction of CD20 $^+$ B cells (green arrowhead) ($N = 2$); magnification 400 \times scale bar 50 μ m. **(e)** Representative PD-L1 $^+$ (upper row) and PD-L1 $^-$ (lower row) LSCC cases with absence of PD-L1 reactivity on PAX5 $^+$ B cells ($N = 4$), magnification 400 \times scale bar 50 μ m.

that B cells contribute selectively to the anti-tumor response in the context of mature TLS, whereas the extra-TLS component likely promotes immunosuppression.^{49,50}

The existence of immunosuppressive and tumor-promoting B cells (Bregs) was first described in the 1990s^{51,52} in the mouse system. The most studied population is characterised by the B10 phenotype, identified by Yanaba et al.⁵³ and subsequently confirmed in human solid tumors.^{54,55} B10 cells (CD1d^{hi}CD5⁺CD19⁺) are located in lymphoid organs, express switched (IgM⁻) or unswitched (IgM⁺) B-memory (CD27⁺) phenotype⁵⁶ and produce IL-10.^{55,57}

Several studies have reported the crucial role of IL-10 in B-cell regulation.⁴⁸ However, IL-10-independent regulatory functions were identified as mediated by TGFβ.⁵⁸ Preclinical studies indicate that a population of TGFβ⁺ Bregs can be generated starting from a pool of naïve B-cells exposed to tumor-derived factors, such as exosomes,⁵⁹ in agreement with the observed mature naïve phenotype of TIB in the context of LSCC (BCL6⁻, CD27⁻ and Mum1⁻).

The subset of Bregs, also referred as tumor-evoked Bregs (tBregs),³⁶ was identified in both the murine and solid tumor models by Olkhanud et al.,³⁶ and its properties and phenotype are consistent with the TIB identified above described in the LSCC patients in our study (CD20⁺, PAX1⁺, CD27⁻, Mum1⁻, IL10⁻, TGFβ⁺, FOXP3⁻, PD-L1⁻). The tBreg regulatory functions are IL-10-independent; by secreting TGFβ, they promote FOXP3⁺ Treg^{36,60} conversion. Furthermore, by flow cytometry, the tBreg phenotype was described as mature B2 CD19⁺pSTAT3⁺CD81^{hi}CD25⁺CD27⁻IgD⁺ and the results from a breast cancer mouse model support their key role in promoting cancer metastasis.^{36,60}

Given the occurrence of Breg populations in the immune contexture of solid tumors, the therapeutic benefit of the depletion of the B cells has been tested with rituximab. However, the results were disappointing and the treatment greatly enhanced cancer progression and metastasis.⁶¹ In contrast, the positive results obtained in the murine models targeting the TGFβ pathway paved the way for the design of clinical trials in human solid tumors.^{62,63} Despite the fact that several molecules targeting the TGFβ pathway were designed and multiple trials conducted in the last 15 years, there is still no clinical approval of these compounds beyond

clinical trials.^{63,64} As these drugs do not exert a direct cytotoxic effect on cancer cells, ongoing studies are testing the best clinical scenarios (i.e. drug combinations and biomarkers of response). Of note, in the HNSCC field, the Bintrafusp alfa (M7824) molecule, with a combined target effect on TGFβ and PD-L1, has shown promising preliminary results with an objective response rate ranging from 13% to 30.5%, with the highest observed in HPV-related tumors.^{63,65,66} Currently, M7824 is under investigation in trial NCT04220775 (NCT number), combined with stereotaxic radiotherapy in recurrent or second primary HNSCCs, and definitive results in the neoadjuvant setting – from trials NCT04247282 and NCT04428047, whose enrollments are already completed – are expected within 1 year.

In terms of biomarkers of response, a rationale exists for pSMAD2 expression⁶³ as detected in the nucleus of LSCC cells and surrounding stroma cells. The SMAD-dependent TGFβ pathways shape the protumoral trajectory in various cancer types also by instructing various immune cells.^{67,68} In our series, the evidence of diffuse positivity of pSMAD2 on both TIBs and tumor cells supports the rationale of considering this pathway active and targetable in the clinical context of LSCC.⁶³

In conclusion, this work identifies a subset of TIBs likely promoting recurrence in the distant control of LSCC. These preliminary findings require additional validation on LSCC and extension to other cancer types producing TGFβ.

METHODS

Study design and cohort of patients

The study is a retrospective and translational study, retrieving clinical data and pathologic specimens from a homogeneous cohort of patients affected by LSCC and treated at the Otorhinolaryngology Unit at the IRCCS Ospedale Policlinico San Martino, University of Genoa, Italy (IRB approval: CER Liguria 230/2019).

As inclusion criteria, we enrolled patients affected by intermediate to advanced T-category LSCC that had undergone surgery as primary treatment between 2012 and 2016, with at least 12 months of follow-up or earlier death or recurrence. Early T-stage tumors (T1 category), salvage surgery, metastatic disease or prior systemic treatment for malignancy were exclusion criteria. Patients were monitored regularly with clinical examinations and neck MRI or CT every 3–6 months. For pTNM staging, the 8th ed. of TNM was applied.³⁹ Surgical procedures included TLM, OPHL or TL. Patients with clinically positive nodes, with high-risk features or who underwent open neck surgery, were

subjected to lateral and central compartment neck dissection. Patients affected by advanced staged tumors, with high-risk features such as PNI, vascular invasion, multiple positive lymph nodes or positive margin, were treated with adjuvant radiotherapy or chemoradiotherapy, following the NCCN guidelines.⁶⁹ Clinical and pathological data taken into account included the following: age, gender, smoke and alcohol consumption, site of the neoplasm, type of treatment, pT category, pN category, overall Stage, Grading, Cartilage invasion (cricoid or thyroid), laryngeal motility, extranodal extension for positive lymph nodes, surgical margins (negative or positive) and follow-up data. The LRF5 rate, the distant recurrence-free survival rate (DRFS), the overall survival rate (OS) and the disease-specific survival rate (DSS) were considered as survival end points, defined as the time between surgery and the date of the corresponding event (locoregional recurrence, distant metastasis, death for any cause, cancer-related death) or censoring at the last follow-up. Details of the cohort are reported in Table 1.

Immunohistochemical staining

Immunohistochemistry (IHC) was performed on a set of tissues samples obtained from the archive of the Department of Pathology (Policlinico San Martino, Genova). For each patient, tissues included a representative whole-tissue formalin-fixed, paraffin-embedded (FFPE) block of primary carcinoma. Immunostaining was performed using 4 μm -thick tissue sections and a set of primary antibodies (Supplementary table 1).

The reaction was revealed using Novolink Polymer (Leica Microsystems) followed by diaminobenzidine (DAB, Dako, Glostrup, Denmark). Finally, the slides were counterstained with Meyer's Haematoxylin.

For double staining, after completing the first immune reaction, the second was visualised using Mach 4 MR-AP (Biocare Medical), followed by Ferangi Blue (Biocare Medical). For triple IHC, the third immune reaction was revealed using Novolink Polymer (Leica Microsystems), and developed in 3-amino-9-ethylcarbazole chromogen (AEC), counterstained with haematoxylin and cover-slipped using gelatin. Single staining for CD3, CD8, CD20, CD66b, CD163 and CD38 was applied to identify T cells, B cells, neutrophils, macrophages and plasma cells, respectively. To characterise the phenotype and the localisation of tumor-associated B cells, we performed double and triple immunostaining for a set of B-cell markers including CD20, BCL6, CD27, PAX5, MUM1, CD38, FOXP3, PD-L1 and pSMAD2.

Digital microscopy analysis

The CD3, CD8, CD20, CD66b, CD163 and CD38 stained slides were digitalised using the Aperio CS2 digital scanner and ScanScope software (Aperio Technologies, Leica Biosystem, New Castle Ltd, UK) at 20 \times magnification and analysed using ImageScope (Leica Microsystems). Each scanned image was annotated manually, and IHC Nuclear Image Analysis algorithm or V9-pixel count algorithm (Leica Biosystems, New Castle Ltd, UK) was chosen for the computerised

whole slide analysis. From each case, we obtained the quantitative measure of immune cell density (number of cells mm^{-2} or the relative frequency of the area positive for the biomarker) for the entire tumor area, including the invasive margin of the tumor, the latter considered to be an area 500 μm wide beneath the tumor nests. Examples of counted fields are provided in Supplementary table 1. For each section stained for CD20, these cells were also organised into aggregates also identifiable as tertiary lymphoid structures, based on the occurrence of BCL6⁺ germinal centre B cells and localisation in the same region of T cells, seen on the serial section stained for CD3 (CD20^{TL5}) or in form of diffuse stromal/intratymoral infiltrate (CD20^{IT}). The density of CD20^{IT} (number of CD20⁺ cells mm^{-2}) was measured, excluding the aggregates of B cells and the TLS density (number of TLS mm^{-2}).

RNAscope

To localise IL10- and TGF β -positive cells, the tissues were analysed with RNAscope assay (Advanced Cell Diagnostics, Newark, CA, USA) using RNAscope 2.5 HD Assay-RED kit, Hs-IL10 probe (cat. no. 602051) recognising the nt 122–1163 of the IL10 reference sequence NM_000572.2 and Hs-TGF β probe (cat. no. 400881) recognising the nt 170–1649 of the TGF β reference sequence NM_000660.4. The sections from fixed human tissue blocks were treated following the manufacturer's instructions. Briefly, freshly cut 3- μm sections were deparaffinised in xylene and treated with the peroxidase block solution for 10 min at room temperature followed by the retrieval solution for 15 min at 98 °C and by protease plus at 40 °C for 30 min. Control probes included Hs-PPIB (cat. no. 313901) and DapB (cat. no. 310043). The hybridisation was performed for 2 h at 40 °C. The signal was revealed using RNAscope 2.5 HD Detection Reagent-RED. Combined RNAscope and immunohistochemistry (for CD20, CD163, CD66b, SMA) were used to identify the cellular source of IL10- and TGF β -positive cells. To this end, IL10 and TGF β detection by RNAscope was followed by immunoreaction visualised using Mach 4 MR-AP (Biocare Medical) followed by Ferangi Blue (Biocare Medical).

Cell-block preparation

Cell suspensions of monocyte-derived macrophages (MDM) were centrifuged for 10 min at 282 *g*. A solution of plasma (100 μL , kindly provided by Centro Trasfusionale, ASST Spedali Civili, Brescia) and HemosIL8 RecombiPlasTin 2G (200 μL , Instrumentation Laboratory, Bedford, MA, USA, cat. no. 0020003050) (1:2) were added to cell pellets, mixed until the formation of a clot, and then placed into a labelled cassette. The specimen was fixed in 10% formalin for 1 h followed by paraffin inclusion.

Real-time PCR

IL-10 and TGF β mRNA targets were quantified by reverse transcription-polymerase chain reaction (qRT-PCR) assay using the Vii-A 7 Real-Time PCR System (Applied Biosystems, Thermo Fisher Scientific, Waltham, MA, USA). Total RNA

was purified from M0, M1 and M2 macrophages ($n = 1$), as previously reported.⁷⁰ The cDNA was synthesised by iScript gDNA cDNA Synthesis kit (cat. no. 1725035; Biorad, Hercules, CA, USA) from 500 ng of total RNA, in a total volume of 20 μ L. A volume of 1 μ L of the cDNA synthesis reaction was used for the specific amplification of the target transcripts. The HPRT1 transcript was used as normalisation control. The qPCR was performed in a total volume of 10 μ L with TaqMan® Universal Master Mix II (cat. no. 4369016; Applied Biosystems, Thermo Fisher Scientific) and the Gene Expression Assay for IL10 (Hs00961622-m1), TGF β 1 (Hs00998133-m1) and HPRT1 (cat. no. 4333768T; Applied Biosystems, Thermo Fisher Scientific). The threshold cycle (Ct) was determined for each sample and quantification was performed using the comparative $\Delta\Delta$ Ct method:

Δ Ct was derived from

$$Ct_{\text{Target}} - Ct_{\text{Housekeeping}}$$

then $\Delta\Delta$ Ct was derived from

$$\Delta Ct_{\text{Target sample (M1}\phi \text{ or M2}\phi)} - \Delta Ct_{\text{Control sample (M0}\phi)}$$

Statistical analysis

Standard descriptive statistics were used for data summarising and expressing means, medians, interquartile range and ranges. The Shapiro–Wilk test was applied to verify the normality of continuous variable distribution. Missing values of clinical variables were imputed with Multivariate Imputation by Chained Equations (MICE).⁷¹

Correlation analysis between immune cells densities was performed using nonparametric Spearman's rank correlation. The Wilcoxon–Mann–Whitney test or Kruskal–Wallis test (followed by Bonferroni P -value adjustment) were used for group comparisons in quantitative variables, and Fisher's exact test for qualitative variables, as appropriate. For achieving a qualitative description of cohabiting immune cells, an Exact Barnes–Hut t-Distributed Stochastic Neighbor Embedding (tSNE) was computed considering Z-scored immune cell infiltration, with Euclidean distance used to measure similarity.⁷²

The median follow-up time was estimated using the reverse Kaplan–Meier method. Multivariable semiparametric Cox proportional hazards models – presented for each outcome – were built by estimating the linear predictors of the full models (including all candidate predictors) and developing simplified models that can predict the values of the full model with high accuracy ($R^2 \geq 0.85$). The simplification employed an Akaike's Information Criterion (AIC) guided fast backward stepdown against the full model predicted values. Each model was validated internally using bootstrap with 300 resamples. Discrimination was measured by the concordance index (c-index), reported as naive model estimates, its bootstrap estimate (average of individual bootstrap estimates) and optimism-corrected estimate.

For clustering analysis, we chose the optimum number of clusters for subdividing the cohort into groups according to the Z-scored immune cells infiltration, by applying the average silhouette method.⁷³ Cluster partitioning was performed applying the k -means algorithm with 1000

repetitions. A heatmap was built for graphical evaluation of the results. Comparisons of clusters have been performed by Fisher's exact test or the Wilcoxon–Mann–Whitney test.

In all the analyses, the significance level was 5%. R (version 4.0.2) and R studio was used for statistical analysis.

ACKNOWLEDGMENTS

WV is funded by the Associazione Italiana per la Ricerca sul Cancro (AIRC-IG-23179). Open access funding provided by BIBLIOSAN.

CONFLICT OF INTEREST

The authors declare no conflict of interest.

AUTHOR CONTRIBUTIONS

Francesco Missale: Conceptualization; data curation; formal analysis; investigation; methodology; supervision; validation; visualization; writing – original draft; writing – review and editing. **Mattia Bugatti:** Data curation; investigation; methodology; validation; visualization. **Filippo Marchi:** Conceptualization; methodology; writing – review and editing. **Giulio E Mandelli:** Data curation; investigation; methodology. **Maria Bruni:** Data curation; investigation; methodology; visualization. **Giulia Palmerini:** Data curation; investigation; methodology; validation; visualization. **Matilde Monti:** Formal analysis; investigation; methodology; validation; writing – review and editing. **Anna M Bozzola:** Investigation; methodology; visualization. **Giorgio Arena:** Data curation; investigation. **Luca Guastini:** Resources; supervision. **Maurizio Boggio:** Investigation; methodology. **Giampiero Parrinello:** Data curation; investigation. **Giorgio Peretti:** Conceptualization; project administration; resources; supervision; writing – review and editing. **William Vermi:** Conceptualization; funding acquisition; investigation; project administration; resources; supervision; validation; visualization; writing – review and editing.

DATA AVAILABILITY STATEMENT

The full data set is available at: 'Larynx_GE_TILS_Dataset', Mendeley Data, V1, <https://doi.org/10.17632/zgp6yt5s2m.1> (Embargo date: 5 May 2023).

REFERENCES

- Dunn GP, Old LJ, Schreiber RD. The three Es of cancer immunoediting. *Annu Rev Immunol* 2004; **22**: 329–360.
- Mittal D, Gubin MM, Schreiber RD, Smyth MJ. New insights into cancer immunoediting and its three component phases—elimination, equilibrium and escape. *Curr Opin Immunol* 2014; **27**: 16–25.
- Koebel CM, Vermi W, Swann JB et al. Adaptive immunity maintains occult cancer in an equilibrium state. *Nature* 2007; **450**: 903–907.

4. Dunn GP, Bruce AT, Ikeda H, Old LJ, Schreiber RD. Cancer immunoediting: from immunosurveillance to tumor escape. *Nat Immunol* 2002; **3**: 991–998.
5. Teng MWL, Ngiew SF, Ribas A, Smyth MJ. Classifying cancers based on T-cell infiltration and PD-L1. *Cancer Res* 2015; **75**: 2139–2145.
6. Galon J, Costes A, Sanchez-Cabo F et al. Type, density, and location of immune cells within human colorectal tumors predict clinical outcome. *Science* 2006; **313**: 1960–1964.
7. Bindea G, Mlecnik B, Tosolini M et al. Spatiotemporal dynamics of intratumoral immune cells reveal the immune landscape in human cancer. *Immunity* 2013; **39**: 782–795.
8. Fridman WH, Pages F, Sautès-Fridman C, Galon J. The immune contexture in human tumors: impact on clinical outcome. *Nat Rev Cancer* 2012; **12**: 298–306.
9. Fridman WH, Zitvogel L, Sautès-Fridman C, Kroemer G. The immune contexture in cancer prognosis and treatment. *Nat Rev Clin Oncol* 2017; **14**: 717–734.
10. Grivas P, Monk BJ, Petrylak D et al. Immune checkpoint inhibitors as switch or continuation maintenance therapy in solid tumors: rationale and current state. *Target Oncol* 2019; **14**: 505–525.
11. Ferris RL, Blumenschein GJ, Fayette J et al. Nivolumab for recurrent squamous-cell carcinoma of the head and neck. *N Engl J Med* 2016; **375**: 1856–1867.
12. Cohen EEW, Soulières D, Le Tourneau C et al. Pembrolizumab versus methotrexate, docetaxel, or cetuximab for recurrent or metastatic head-and-neck squamous cell carcinoma (KEYNOTE-040): a randomised, open-label, phase 3 study. *Lancet* 2019; **393**: 156–167.
13. Mehra R, Seiwert TY, Gupta S et al. Efficacy and safety of pembrolizumab in recurrent/metastatic head and neck squamous cell carcinoma: pooled analyses after long-term follow-up in KEYNOTE-012. *Br J Cancer* 2018; **119**: 153–159.
14. Schoenfeld JD, Hanna GJ, Jo VY et al. Neoadjuvant nivolumab or nivolumab plus ipilimumab in untreated oral cavity squamous cell carcinoma: a phase 2 open-label randomized clinical trial. *JAMA Oncol* 2020; **6**: 1563–1570.
15. Horton JD, Knochelmann H, Armeson K, Kaczmar JM, Paulos C, Neskey D. Neoadjuvant presurgical PD-1 inhibition in oral cavity squamous cell carcinoma. *J Clin Oncol* 2019; **37**: 2574.
16. Saito S, Shibata H, Adkins D, Uppaluri R. Neoadjuvant immunotherapy strategies in HPV-related head-and-neck cancer. *Curr Otorhinolaryngol Rep* 2022; **10**: 108–115.
17. Vos JL, Elbers JBW, Krijgsman O et al. Neoadjuvant immunotherapy with nivolumab and ipilimumab induces major pathological responses in patients with head and neck squamous cell carcinoma. *Nat Commun* 2021; **12**: 7348.
18. Lawrence MS, Sougnez C, Lichtenstein L et al. Comprehensive genomic characterization of head and neck squamous cell carcinomas. *Nature* 2015; **517**: 576–582.
19. Mandal R, Şenbabaoglu Y, Desrichard A et al. The head and neck cancer immune landscape and its immunotherapeutic implications. *JCI Insight* 2016; **1**: e89829.
20. Vaculik MF, MacKay CA, Taylor SM, Trites JRB, Hart RD, Rigby MH. Systematic review and meta-analysis of T1 glottic cancer outcomes comparing CO₂ transoral laser microsurgery and radiotherapy. *J Otolaryngol Head Neck Surg* 2019; **48**: 44.
21. Hoffman HT, Porter K, Karnell LH et al. Laryngeal cancer in the United States: changes in demographics, patterns of care, and survival. *Laryngoscope* 2006; **116**: 1–13.
22. Vermorken JB, Mesia R, Rivera F et al. Platinum-based chemotherapy plus cetuximab in head and neck cancer. *N Engl J Med* 2008; **359**: 1116–1127.
23. Duprez F, Berwouts D, De Neve W et al. Distant metastases in head and neck cancer. *Head Neck* 2017; **39**: 1733–1743.
24. Zhou L, Li Y, Gao W et al. Assessment of tumor-associated immune cells in laryngeal squamous cell carcinoma. *J Cancer Res Clin Oncol* 2019; **145**: 1761–1772.
25. Höing B, Kanaan O, Altenhoff P et al. Stromal versus tumoral inflammation differentially contribute to metastasis and poor survival in laryngeal squamous cell carcinoma. *Oncotarget* 2018; **9**: 8415–8426.
26. Karpathiou G, Casteillo F, Giroult JB et al. Prognostic impact of immune microenvironment in laryngeal and pharyngeal squamous cell carcinoma: immune cell subtypes, immuno-suppressive pathways and clinicopathologic characteristics. *Oncotarget* 2017; **8**: 19310–19322.
27. Hoesli R, Birkeland AC, Rosko AJ et al. Proportion of CD4 and CD8 tumor infiltrating lymphocytes predicts survival in persistent/recurrent laryngeal squamous cell carcinoma. *Oral Oncol* 2018; **77**: 83–89.
28. Zhang D, Tang D, Heng Y et al. Prognostic impact of tumor-infiltrating lymphocytes in laryngeal squamous cell carcinoma patients. *Laryngoscope* 2021; **131**: e1249–e1255.
29. Chatzopoulos K, Kotoula V, Manoussou K et al. Tumor infiltrating lymphocytes and CD8⁺ T cell subsets as prognostic markers in patients with surgically treated laryngeal squamous cell carcinoma. *Head Neck Pathol* 2020; **14**: 689–700.
30. Lonardi S, Missale F, Calza S et al. Tumor-associated neutrophils (TANs) in human carcinoma-draining lymph nodes: a novel TAN compartment. *Clin Transl Immunology* 2021; **10**: e1252.
31. El-Naggar AK, Chan JKC, Grandis JR, Takata T, Slootweg PJ. *WHO Classification of Head and Neck Tumors*. Lyon: International Agency for Research on Cancer (IARC); 2017.
32. Wondergem NE, Nauta IH, Muijlwijk T, Leemans CR, van de Ven R. The immune microenvironment in head and neck squamous cell carcinoma: on subsets and subsites. *Curr Oncol Rep* 2020; **22**: 81.
33. Wieland A, Patel MR, Cardenas MA et al. Defining HPV-specific B cell responses in patients with head and neck cancer. *Nature* 2021; **597**: 274–278.
34. Wang S-S, Liu W, Ly D, Xu H, Qu L, Zhang L. Tumor-infiltrating B cells: their role and application in anti-tumor immunity in lung cancer. *Cell Mol Immunol* 2019; **16**: 6–18.

35. Rekhtman N, Bishop JA. *Quick Reference Handbook for Surgical Pathologists*. Berlin, Heidelberg: Springer; 2011.
36. Olkhanud PB, Damdinsuren B, Bodogai M et al. Tumor-evoked regulatory B cells promote breast cancer metastasis by converting resting CD4⁺ T cells to T-regulatory cells. *Cancer Res* 2011; **71**: 3505–3515.
37. Catalán D, Mansilla MA, Ferrier A et al. Immunosuppressive mechanisms of regulatory B cells. *Front Immunol* 2021; **12**: 611795.
38. Pages F, Berger A, Camus M et al. Effector memory T cells, early metastasis, and survival in colorectal cancer. *N Engl J Med* 2005; **353**: 2654–2666.
39. Amin MB, Edge SB. *AJCC Cancer Staging Manual*. Cham, CH: Springer International Publishing; 2017.
40. Lin J-Y, Li X-Y, Tadashi N, Dong P. Clinical significance of tumor-associated macrophage infiltration in supraglottic laryngeal carcinoma. *Chin J Cancer* 2011; **30**: 280–286.
41. Mann JE, Smith JD, Birkeland AC et al. Analysis of tumor-infiltrating CD103 resident memory T-cell content in recurrent laryngeal squamous cell carcinoma. *Cancer Immunol Immunother* 2019; **68**: 213–220.
42. Rodrigo JP, Sánchez-Canteli M, López F et al. Tumor-infiltrating lymphocytes in the tumor microenvironment of laryngeal squamous cell carcinoma: systematic review and meta-analysis. *Biomedicines* 2021; **9**: 486.
43. Becht E, Giraldo NA, Beuselinck B et al. Prognostic and theranostic impact of molecular subtypes and immune classifications in renal cell cancer (RCC) and colorectal cancer (CRC). *Onco Targets Ther* 2015; **4**: e1049804.
44. Giraldo NA, Becht E, Vano Y et al. Tumor-infiltrating and peripheral blood T-cell immunophenotypes predict early relapse in localized clear cell renal cell carcinoma. *Clin Cancer Res* 2017; **23**: 4416–4428.
45. Sorrentino C, D'Antonio L, Fieni C, Ciunmo SL, Di Carlo E. Colorectal cancer-associated immune exhaustion involves T and B lymphocytes and conventional NK cells and correlates with a shorter overall survival. *Front Immunol* 2021; **12**: 778329.
46. Zhang Y, Li L, Zheng W, Zhang L, Yao N. CD8⁺ T-cell exhaustion in the tumor microenvironment of head and neck squamous cell carcinoma determines poor prognosis. *Ann Transl Med* 2022; **10**: 273.
47. Alfieri S, Carezzo A, Platini F et al. Tumor biomarkers for the prediction of distant metastasis in head and neck squamous cell carcinoma. *Cancers (Basel)* 2020; **12**: e922.
48. Wang L, Fu Y, Chu Y. Regulatory B cells. *Adv Exp Med Biol* 2020; **1254**: 87–103.
49. Cabrita R, Lauss M, Sanna A et al. Tertiary lymphoid structures improve immunotherapy and survival in melanoma. *Nature* 2020; **577**: 561–565.
50. Kinker GS, Vitiello GAF, Ferreira WAS, Chaves AS, Cordeiro de Lima VC, Medina TS. B cell orchestration of anti-tumor immune responses: a matter of cell localization and communication. *Front Cell Dev Biol* 2021; **9**: 678127.
51. Wolf SD, Dittel BN, Hardardottir F, Janeway CA. Experimental autoimmune encephalomyelitis induction in genetically B cell-deficient mice. *J Exp Med* 1996; **184**: 2271–2278.
52. Mizoguchi A, Mizoguchi E, Smith RN, Preffer FI, Bhan AK. Suppressive role of B cells in chronic colitis of T cell receptor alpha mutant mice. *J Exp Med* 1997; **186**: 1749–1756.
53. Yanaba K, Bouaziz J-D, Matsushita T, Tsubata T, Tedder TF. The development and function of regulatory B cells expressing IL-10 (B10 cells) requires antigen receptor diversity and TLR signals. *J Immunol* 2009; **182**: 7459–7472.
54. Mao Y, Wang Y, Dong L et al. Circulating exosomes from esophageal squamous cell carcinoma mediate the generation of B10 and PD-1^{high} Breg cells. *Cancer Sci* 2019; **110**: 2700–2710.
55. DiLillo DJ, Matsushita T, Tedder TF. B10 cells and regulatory B cells balance immune responses during inflammation, autoimmunity, and cancer. *Ann NY Acad Sci* 2010; **1183**: 38–57.
56. Mehdipour F, Razmkhah M, Faghieh Z, Bagheri M, Talei A-R, Ghaderi A. The significance of cytokine-producing B cells in breast tumor-draining lymph nodes. *Cell Oncol (Dordr)* 2019; **42**: 381–395.
57. Mauri C, Bosma A. Immune regulatory function of B cells. *Annu Rev Immunol* 2012; **30**: 221–241.
58. Teichmann LL, Kashgarian M, Weaver CT, Roers A, Müller W, Shlomchik MJ. B cell-derived IL-10 does not regulate spontaneous systemic autoimmunity in MRL.Fas^{lpr} mice. *J Immunol* 2012; **188**: 678–685.
59. Han S, Feng S, Ren M et al. Glioma cell-derived placental growth factor induces regulatory B cells. *Int J Biochem Cell Biol* 2014; **57**: 63–68.
60. Biragyn A, Lee-Chang C, Bodogai M. Generation and identification of tumor-evoked regulatory B cells. *Methods Mol Biol* 2014; **1190**: 271–289.
61. Bodogai M, Lee Chang C, Wejksza K et al. Anti-CD20 antibody promotes cancer escape via enrichment of tumor-evoked regulatory B cells expressing low levels of CD20 and CD137L. *Cancer Res* 2013; **73**: 2127–2138.
62. Morris JC, Tan AR, Olencki TE et al. Phase I study of GC1008 (fresolimumab): a human anti-transforming growth factor-beta (TGFβ) monoclonal antibody in patients with advanced malignant melanoma or renal cell carcinoma. *PLoS One* 2014; **9**: e90353.
63. Ciardiello D, Elez E, Tabernero J, Seoane J. Clinical development of therapies targeting TGFβ: current knowledge and future perspectives. *Ann Oncol* 2020; **31**: 1336–1349.
64. Liu S, Ren J, Ten Dijke P. Targeting TGFβ signal transduction for cancer therapy. *Signal Transduct Target Ther* 2021; **6**: 8.
65. Cho BC, Daste A, Ravaut A et al. Bintrafusp alfa, a bifunctional fusion protein targeting TGF-β and PD-L1, in advanced squamous cell carcinoma of the head and neck: results from a phase I cohort. *J Immunother Cancer* 2020; **8**: e000664.
66. Strauss J, Gatti-Mays ME, Cho BC et al. Bintrafusp alfa, a bifunctional fusion protein targeting TGF-β and PD-L1, in patients with human papillomavirus-associated malignancies. *J Immunother Cancer* 2020; **8**: e001395.
67. Chan MK-K, Chung JY-F, Tang PC-T et al. TGF-β signaling networks in the tumor microenvironment. *Cancer Lett* 2022; **550**: 215925.
68. Batlle E, Massagué J. Transforming growth factor-β signaling in immunity and cancer. *Immunity* 2019; **50**: 924–940.

69. Pfister D, Spencer S, Adelstein D. *NCCN Guidelines Version 3.2019 Head and Neck Cancers*. 2019.
70. Ardighieri L, Missale F, Bugatti M *et al.* Infiltration by CXCL10 secreting macrophages is associated with antitumor immunity and response to therapy in ovarian cancer subtypes. *Front Immunol* 2021; **12**: 690201.
71. van Buuren S, Groothuis-Oudshoorn K. mice: multivariate imputation by chained equations in R. *J Stat Softw* 2011: 1–67. <https://www.jstatsoft.org/v045/i03>
72. Van der Maaten L, Hinton G. Visualizing data using t-SNE. *J Mach Learn Res* 2008; **9**: 2579–2605.
73. Gentle JE, Kaufman L, Rousseuw PJ. Finding groups in data: an introduction to cluster analysis. *Biometrics* 1991; **47**: 788.

Supporting Information

Additional supporting information may be found online in the Supporting Information section at the end of the article.



This is an open access article under the terms of the [Creative Commons Attribution-NonCommercial-NoDerivs](#) License, which permits use and distribution in any medium, provided the original work is properly cited, the use is non-commercial and no modifications or adaptations are made.